UC Davis
UC Davis Previously Published Works

Title

Alterations in Retrotransposition, Synaptic Connectivity, and Myelination Implicated by Transcriptomic Changes Following Maternal Immune Activation in Nonhuman Primates

Permalink

https://escholarship.org/uc/item/67c529mv

Journal

Biological Psychiatry, 89(9)

ISSN

0006-3223

Authors

Page, Nicholas F
Gandal, Michael J
Estes, Myka L
et al.

Publication Date

2021-05-01

DOI

10.1016/j.biopsych.2020.10.016

Peer reviewed

Alterations in retrotransposition, synaptic connectivity, and myelination implicated by transcriptomic changes following maternal immune activation in non-human primates

Nicholas F. Page[#],(1),(2), Michael Gandal[#],(1), Myka Estes(3), Scott Cameron(3), Jessie Buth(1),(4), Sepideh Parhami(1),(4), Gokul Ramaswami(1),(4), Karl Murray(5), David G. Amaral(5), Judy A. Van de Water(5), Cynthia M. Schumann(5), Cameron S. Carter(3),(5), Melissa D. Bauman(5), A. Kimberley McAllister(3),(5), Daniel H. Geschwind(1),(4),(6),(7)

[1]Department of Psychiatry, Semel Institute, David Geffen School of Medicine, University of California Los Angeles, 695 Charles E. Young Drive South, Los Angeles, CA 90095, USA.

[2]Department of Cell Biology and Neuroscience, Rutgers University-New Brunswick, Piscataway, NJ 08854.

[3]Center for Neuroscience, University of California Davis, One Shields Avenue, Davis, CA 95616, USA.

[4]Program in Neurobehavioral Genetics, Semel Institute, David Geffen School of Medicine, University of California, Los Angeles, Los Angeles, CA 90095, USA.

[5]Department of Psychiatry and Behavioral Sciences, School of Medicine, University of California, Davis, Sacramento, CA 95817.

[6]Department of Neurology, Center for Autism Research and Treatment, Semel Institute, David Geffen School of Medicine, University of California, Los Angeles, 695 Charles E. Young Drive South, Los Angeles, CA 90095, USA.

[7]Department of Human Genetics, David Geffen School of Medicine, University of California, Los Angeles, Los Angeles, CA 90095, USA.

Abstract

Background: Maternal immune activation (MIA) is a proposed risk factor for multiple neuropsychiatric disorders, including schizophrenia. However, the molecular mechanisms through which MIA imparts risk remain poorly understood. A recently developed nonhuman primate model of exposure to the viral mimic poly:ICLC during pregnancy shows abnormal social and

Corresponding Author Daniel H. Geschwind, 2506 Gonda Building, 695 Charles E. Young Dr. South, Los Angeles, CA 90095-1761, dhg@mednet.ucla.edu, Phone: (310) 794-6570.
[#]Co-first authors.

repetitive behaviors and elevated striatal dopamine, a molecular hallmark of human psychosis, providing an unprecedented opportunity for studying underlying molecular correlates.

Methods: We performed RNA-sequencing across psychiatrically relevant brain regions (prefrontal cortex, anterior cingulate, hippocampus) and primary visual cortex for comparison from 3.5–4-year old male MIA-exposed and control offspring—an age comparable to mid adolescence in humans.

Results: We identify 266 unique genes differentially expressed (DE) in at least one brain region with the greatest number observed in hippocampus. Co-expression networks identified region-specific alterations in synaptic signaling and oligodendrocytes. Although we observed temporal and regional differences, transcriptomic changes were shared across 1st and 2nd trimester exposures, including for the top DE genes—*PIWIL2* and *MGARP*. In addition to *PIWIL2*, several other regulators of retrotransposition and endogenous transposable elements were dysregulated following MIA, potentially connecting MIA to retrotransposition.

Conclusions: Together, these results begin to elucidate the brain-level molecular processes through which MIA may impart risk for psychiatric disease.

Introduction

Epidemiological studies have implicated *in utero* environmental insults, including maternal infections, as risk factors for neurodevelopmental disorders, such as schizophrenia (SCZ) and autism spectrum disorder (ASD) (1–7). These results are in accordance with twin and family studies, which have demonstrated that early childhood environmental factors contribute to liability for SCZ (8). The wide range of infectious agents and exposures reported in the clinical literature suggests that common factors downstream of the maternal immune response may confer risk (7). However, it remains unclear how maternal infection alters brain development in offspring to increase risk for neurodevelopmental disorders.

To investigate this hypothesis, animal models of maternal immune activation (MIA) were developed using the viral mimic, poly(I:C) (9). Multiple laboratories have developed rodent models that exhibit reproducible behavioral phenotypes in domains altered in human psychiatric illness (1, 9–14). These rodent MIA models also exhibit neuropathological alterations similar to those found in neuropsychiatric disorders (11–13, 15–21) and several of the behavioral aberrations are rescued by antipsychotics (11–13, 22–25). Recently, a non-human primate (NHP) model of MIA was developed, whose young adult offspring display abnormalities in communication, decreased social attention and interaction, and increased stereotypic behaviors that increase in intensity with age (10–13, 26, 27). NHP MIA offspring also show a molecular hallmark of psychosis—enhanced striatal dopamine, similar to the increases seen in SCZ (28). While behavioral changes have been well characterized, as have molecular alterations in rodents, the field still lacks an understanding of the molecular changes associated with MIA in NHPs that may underlie these behaviors.

Transcriptomic tools such as RNA-seq have revealed substantial changes in disease (29, 30) and enable unbiased systematic characterization of the brain level molecular changes underlying behavioral phenotypes in these models. Transcriptomic alterations have also been detected in adult mice following MIA including changes in myelination (31), mTOR signaling and potassium ion channel activity (32), dopamine related pathways (33), and inflammatory responses in microglia (34). A recent study identified potential overlapping pathways in mouse MIA and human SCZ post mortem brain, suggesting the potential for MIA contribution to human disease (35). It remains unknown, however, to what extent such changes are shared across species.

Here, we conduct the first systematic, multi-regional RNA-seq analysis of the NHP brain following MIA at two timepoints, the 1st and 2nd trimester. We identify 266 unique genes differentially expressed (DE) in at least one brain region in male MIA-exposed offspring, most showing concordant changes across both exposures, including the top DE genes— *PIWIL2* and *MGARP*. Our results reveal altered transposable element biology, dysregulated synaptic connectivity, and enhanced myelination as important molecular pathways underlying the effects of MIA. These findings provide some initial insights into the molecular changes that may precede the onset of psychosis and persist into late adolescence and identify potential targets for future mechanistic dissection.

Methods and Materials

NHP Model of MIA

All animal protocols were developed in conjunction with the California National Primate Research Center and approved by the University of California, Davis Institutional Animal Care and Use Committee. Thirteen female rhesus macaques were split into three treatment conditions: immune activation during the first trimester of pregnancy (1st Trim MIA, n=5), second trimester MIA (2nd Trim MIA, n=4), or control (Ctrl, n=4). The control group consisted of 1 untreated, 1 first trimester saline injected, and 2 second trimester saline injected NHPs. Animals in the MIA conditions were injected intravenously with 0.25 mg/kg of synthetic double-stranded RNA virus (poly:ICLC) (Oncovir, Inc., Washington, DC) on gestational days 43, 44, and 46 (1st Trim MIA) or 100, 101, and 103 (2nd Trim MIA). Animals were housed in the same facility where they had ad libitum access to Lixit-dispensed water, primate laboratory chow was provided twice daily, and fruit and vegetable supplements were provided twice weekly. All animals underwent routine health checks and were assessed twice each day by a trained observer. Any animals observed with clinical signs were assessed by a member of the Primate Medicine Staff and followed up appropriately. Our laboratory observed no differences between MIA and control animals in the frequency or magnitude of common colony infections. Drug exposure for both MIA and control animals was limited to routine medications and/or pharmacological sedation required for treatment and/or physical exams as advised by veterinary staff. Pharmacological sedation was not used for routine animal transport. None of the injected dams in the control group showed any evidence of a maternal immune response. Details of blood IL-6 analysis are in the Supplemental Information.

At 3.5–4 years of age, four brain regions were dissected from the right hemisphere: the dorsolateral prefrontal cortex (DLPFC, BA 9/46) on middle frontal gyrus along the dorsal wall of the principal sulcus, anterior cingulate cortex (ACC, BA24), mid-rostrocaudal hippocampus (HC) caudal to the amygdala, and primary visual cortex (V1). At 3.5–4 years of age, the brain was perfused with saline, extracted, cerebellum and brainstem removed, and cerebrum bisected through the sagittal sulcus into the right and left hemispheres. The right hemisphere was sectioned with a long histology blade into ~9 coronal slabs 6mm thick perpendicular to the anterior-posterior commissural (AC/PC) axis and flash-frozen in liquid nitrogen vapor. Slabs were stored in a −80C freezer until dissection. For further details on animal methods, please see (26).

RNA-sequencing and Analysis

RNA was extracted (Qiagen, miRNA easy-mini), rRNA-depleted RNA-seq libraries were prepared using TruSeq stranded RNA plus ribozero gold kits. Libraries were multiplexed (24 per pool) and sequenced across two batches on an Illumina HiSeq2500 to an average depth of ~50 million 69 bp paired end reads. Reads were mapped to the macaque genome (rheMac8) using the STAR aligner and gene-level quantifications were calculated with Kallisto (36). 6,410 lowly expressed genes were filtered and removed using the filterByExpr method from the R package edgeR and were highly enriched for olfactory receptors and ribosome related genes (Figure S2A). Samples underwent TMM normalization for read depth (37) followed by differential gene expression with Limma-voom (38). Sequencing metrics from Picard Tools were summarized by their top 4 principal components (seqPCs) (Table S1, Supplemental Information), which were included in the linear model to control for batch, RNA quality, and sequencing-related technical effects. As sequencing batch and RNA quality measures (sample 280:260, 260:230 ratios) were strongly correlated with these seqPCs (Figure S1A), they were not included in the final model as covariates. The following model was used, with specific contrast terms to determine DGE between different individual regions: *Expr ~ 0 + Group:Region + seqPCs1–4.* p-values were then corrected for multiple comparisons using the FDRTool package in R. For select genes (e.g. SOX10; Figure 7B) that did not have an annotated homolog in NHPs, RNA-seq reads mapping to annotated human DNA sequences were used to determine expression.

Network Analysis

Network analysis was performed with the WGCNA package (39) using signed networks. A soft-threshold power of 14 was used to achieve approximate scale-free topology ($R2 \cong 0.7$). Networks were constructed using the blockwiseModules function. The network dendrogram was created using average linkage hierarchical clustering of the topological overlap dissimilarity matrix (1-TOM). Modules were defined as branches of the dendrogram using the hybrid dynamic tree-cutting method (39). Modules were summarized by their first principal component (ME, module eigengene) and modules with eigengene correlations of >0.9 were merged together. Modules were defined using biweight midcorrelation (bicor), with a minimum module size of 100, deepsplit of 4, merge threshold of 0.1, and negative pamStage. Module differential expression was determined using a linear model provided by the lmFit function in the Limma package (38). Uncorrected P-values are reported for module differential expression.

Assessment of Retrotransposition and Enrichment Analyses

GO analysis (40), over-representation analysis and Expression Weighted Cell-type Enrichment (EWCE) (41) were performed (see Supplemental Information for details). The RepEnrich2 pipeline (https://github.com/nerettilab/RepEnrich2) was used to estimate repetitive elements in the genome using python version 2.7 (42) as described in the Supplemental Information.

Rank-Rank Hypergeometric Overlap (RRHO)

Original gene lists from this experiment and from studies of post-mortem SCZ and ASD brains were ordered by signed –log10 P-value and compared via a one-sided hypergeometric test with a step size of 100 followed by Benjamini-Yekutieli FDR correction using the *RRHO* package in R (43). Final p-values are reported on a –log10 scale.

Western Blotting

Western blotting was performed using standard methods as described in the Supplemental Information.

Code

Scripts used to perform bioinformatic analyses were written in R and are publicly available on GitHub (https://github.com/dhglab/CONTE_NHP_MIA).

Results

Maternal immune activation induces brain transcriptomic changes in adolescent NHPs

RNA-sequencing was performed on 4 brain regions to characterize brain transcriptomic changes in a well characterized cohort of 3.5–4 year old male non-human primates (NHPs; Figure 1). NHPs were exposed *in utero* to saline or poly:ICLC on 3 days starting at gestational day GD44 (1st Trimester MIA) or GD101 (2nd Trimester MIA; Methods and Materials). Following quality control (Figures 1D, S1, S2A), differential expression (DE) was characterized within and across the brain regions profiled (DLPFC, ACC, HC, and V1) for all 14,975 brain expressed genes detected, which we refer to as regional (individual regions) and global analysis (all regions), respectively (Methods and Materials).

Six genes showed globally significant patterns of differential expression at an FDR < 0.1 -- *PIWIL2*, *MGARP*, *C15orf41*, *SNED1*, *FCRL3*, *RNASE1* (Figure 2A; Table S2). The top DE gene, *PIWIL2*, which is down regulated, is a master regulator of piRNA mediated DNA methylation and an inhibitor of retrotransposition (44, 45). *PIWIL2* also regulates the expression of plasticity-related genes in the adult brain, and disruption of the piwi pathway in HC enhances contextual fear memory in mice (46). The second highest DE gene, *MGARP*, encodes a protein that regulates mitochondrial morphology, distribution, and motility, which when decreased in neurons causes dendritic and axonal overgrowth in mice (47). The other globally significant genes are not well characterized in the brain.

An additional 100 genes showed suggestive global association with MIA (P < 0.005), including several downregulated neurotransmitter receptors (*HTR3A*, *GRIK2*, *GLRA2*) and

the high-confidence SCZ risk gene *AS3MT* (48). Gene ontology enrichment analyses identified significantly up and downregulated terms including *membrane fusion involved in viral entry into host cell* (Figure 2B). Cell-type enrichment analyses (Methods and Materials) indicated that upregulated genes (P < 0.05) were enriched for endothelial cell markers, whereas excitatory neuron (ExN), inhibitory neuron (InN), and oligodendrocyte precursor cell (OPC) markers were enriched among downregulated genes (Figure 2C). These findings demonstrate that MIA-induced changes in brain gene expression affect disease relevant genes, cell-types, and pathways that persist into adolescence in this model.

Specificity of brain molecular changes based on prenatal timing of MIA

In rodent MIA models, the timing of immune activation during pregnancy specifies the nature of neurodevelopmental and behavioral outcomes in affected offspring (1, 14, 49–53). We tested the role of MIA timing on gene expression in the brains of offspring by comparing two susceptibility windows that closely parallel those in humans (54), either 1st or 2nd trimester MIA (Figure 3A; Table S3). None of the control animals injected with saline at either time-point or non-injected had measurable immune activation and therefore were pooled for these comparisons. Transcriptomic changes were largely concordant across timepoints (R of $\log_2$-FC: 0.738, P<10^{-15}) (Figure 3B). *PIWIL2* and *MGARP* emerged as the top downregulated genes during each time point independently. Several genes did show more specific patterns, such as the serotonin receptor *HTR3A* which was significantly downregulated following 1st trimester exposure. In contrast, 2nd trimester exposure showed unique upregulation of *IFITM3*, which mediates the brain immune response to neonatal poly(I:C) exposure and is strongly upregulated in post-mortem brains from subjects with SCZ (55–58). The 2nd trimester signal also showed selective enrichment of RNA processing related gene ontology pathways among downregulated transcripts, indicating that some differences do exist (Figure 3C, D). Given that the global signatures showed significant concordance, we grouped the timepoints together for downstream analyses to boost power.

MIA alters gene expression in the brains of offspring in a region-specific manner

We next compared patterns of DE across distinct regions (Figure 4A), observing the most DE genes in HC (n=118 genes; FDR<0.1), followed by V1 (n=114) and DLPFC (n=34), with only minor DE detected in ACC (Figures 4A, B; Table S2). *PIWIL2* was downregulated in 3 of the 4 regions (DLPFC, ACC, and HC). We relaxed the statistical criterion to detect small, yet concordant transcriptomic changes shared across regions and compared $\log_2$-FC effect sizes for all genes exhibiting suggestive DE (P<0.005) in MIA. The largest correlation ($R = 0.447$; p < 1e-15) was between the DLPFC and ACC and other regions (DLPFC and V1; $R = 0.121$; p = 0.004) appearing more distinct (Figure 4C; Figure S2B). Together, results clearly show that MIA causes DE of genes in a region-specific manner in offspring.

The region-specific effects of MIA also segregate by cell-type and biological process. Upregulated genes in the HC are strongly enriched in oligodendrocytes, whereas downregulated genes are strongly enriched for ExNs, InNs, and OPCs (Figure 4D). Interestingly, the ACC is the only region that contains any cell-type enrichment for microglia

among downregulated genes (Figure 4D). Region specific differences in cell-type enrichment are also concordant with GO term enrichment (Figure 4E).

Convergent gene expression changes following MIA implicate transposition

To more specifically capture the molecular processes underlying transcriptomic changes, we performed weighted gene correlation network analysis (WGCNA), detecting 29 gene co-expression modules (Figure 5A; Figure S2D–E; Table S4). The steelblue module was downregulated across all brain regions (Figure 5B, C) and contained 105 genes, of which 41 lack human homologs. Surprisingly, many of these 41 genes appeared to be associated with transposable element (TE) biology. 8/41 belong to the "LINE-1 RETROTRANSPOSABLE ELEMENT ORF2 PROTEIN" family (PTHR25952:SF231; ref (59)). Other hub genes include *HERV-H LTR-Associating 2* (*HHLA2*), an immune checkpoint molecule, and *Tigger Transposable Element Derived 1* (*TIGD1*), a paralog of centromere binding protein *CENPB* (Figure 5D), both of which were TEs that have evolved into protein coding genes (60). Gene ontology enrichments were observed for pathways related to steroid/lipid metabolism including *INSIG2*, *SULT2A1*, and *FAAH2* (Figure 5E). Notably, only MEsteelblue and the MEyellow module had the same direction of change across all regions (Figure 5F).

After confirming that the top global DE gene, *PIWIL2, was* also downregulated on the protein-level in the HC (Figure 6A–C), we determined whether specific classes of TEs were dysregulated following MIA. Only one specific TE, *HERV1_LTRa*, was detected with an FDR < 0.1 in the ACC while a total of 26 separate TEs had suggestive association with MIA (p < 0.005) in at least one brain region (Supplemental Information; Figure S3A–C). These include multiple elements of the human endogenous retrovirus (HERV) and long terminal repeat (LTR) families of retrotransposons, both of which often modulate transcription (61) (Figure 6D, S3D, E, F). Together, these results indicate specific changes in transposable element biology similar to what has been observed in other neurological diseases as a response to inflammatory signals (62, 63).

Synaptic downregulation and increased myelination in HC

The largest number of DE genes and several unique co-expression modules were observed in the HC (Figures 4A, B, 5F). Upregulated genes in HC showed enrichment for oligodendrocyte and endothelial cell markers, whereas downregulated genes were enriched for excitatory neurons, inhibitory neurons, and oligodendrocyte precursor cells (OPCs) and related GO categories (Figure 4D, E). Synaptic genes included a number of glutamate receptors and high-confidence autism risk genes (Table S2). Additionally, we detected a core up-regulated transcriptomic network important for the differentiation of oligodendrocytes and the production of myelin sheaths including *OLIG2*, *SOX10*, *MYRF*, *PLLP*, *MBP*, *CNP*, *MOG*, and *MAG* (64) (Figure 7A, B). These findings were similarly observed among HC co-expression network modules, including the most significantly up- and downregulated modules, MEturquoise and MEpaleturquoise (Figure 7C, F), enriched for genes related to axon enseathment and neuron projections, respectively (Figure 7D–E, G–H). Other dysregulated co-expression network modules in the HC include MElightgreen which is enriched for "neuron projection development" (Figure 7I–K) and MEtan (Figure 7L–N),

which contains the hub gene *CADPS*, a high confidence autism risk gene involved in synaptic vesicle release (65) (Figure 7M).

Because neuroinflammatory gene expression changes have been reported in SCZ and ASD (30) and cytokines are altered in the mouse MIA brain throughout postnatal development (66), we next examined whether there were modules enriched in glial and immune genes in the NHP model. We did not observe DE in either module enriched for astrocyte (MEgreen) or microglial (MEblue) markers (Figures 5B, F, S4). The lack of a major microglial signature is consistent with recent reports from the MIA mouse model indicating little microglial dysregulation in the brains of adult MIA offspring (67) and from the human literature showing conflicting results from PET imaging studies (68).

Nevertheless, specific examples of immune dysregulation do exist. *CX3CR1* protein, but not mRNA, was significantly downregulated in the DLPFC with no change in HC. *IGSF6* mRNA is trending downwards in both DLPFC and HC, but its protein levels are significantly upregulated in both regions (Figure S6C, D). Differences between mRNA and protein level data suggest compensatory mechanisms at the level of translation and indicate that there are likely protein level immune related changes missed by our current transcriptomic analysis.

Limited overlap in DE genes with SCZ and ASD

The non-human primates examined here (3.5–4 NHP years; 14–16 human equivalent years) are significantly younger than human subjects included in the postmortem analysis for SCZ (median age > 30; refs (30, 54)). Thus, results from the NHP model may provide unique information about the molecular changes that precede the onset of psychosis. We performed a rank-rank hypergeometric overlap test (RRHO) of DE genes in MIA vs ASD or SCZ, detecting no global overlap between the ranked genes from SCZ or ASD and our study (30) (Figures S7A and S7B). However, individual DE genes in multiple brain regions have been linked to ASD or SCZ and downregulated genes from two regions -- HC and V1 -- showed slight enrichment for high-confidence ASD risk genes (SFARI) (Figure S7C).

We also sought to determine whether any gene expression signatures exhibited associations with the increased repetitive, stereotyped behaviors observed following MIA (Figure 8A; Table S5). The total number of stereotypies is weakly correlated with module expression across regions, with the strongest correlations detected in V1. MEmidnightblue and MEdarkorange have the highest correlations with the number of stereotypies ($\log_2$ transformed; $R = 0.64$, P < 0.027; $R = 0.63$, P < 0.027, respectively) (Figure 8B, S8A, S8B). MEmidnightblue displays significant GO enrichment for mitochondrial membrane compartment while MEdarkorange is enriched for mitochondrial compartment, suggesting that cellular respiration in the visual cortex may be loosely associated with repetitive behaviors (Figure 8C–F). MEmidnightblue also displays statistically significant overlap with a mitochondrial gene enriched module (geneM33) from PsychEncode that is downregulated in SCZ and ASD (30) (Figure S8C) and nominally significant overlap with a previously identified mitochondrial co-expression module that is correlated with neuronal activity (69) (Figure S8D).

Finally, we examined whether the severity of maternal interleukin 6 (IL-6) induction following poly:ICLC exposure is correlated with brain molecular phenotypes in our NHP data (Methods and Materials; Table S5). MEdarkorange and MEsalmon in particular have the highest correlation with the measured maternal IL-6 levels ($R = 0.65$; $R = 0.64$ respectively) (Figure S8E). As noted above, MEdarkorange is correlated with increased stereotypies and is enriched for genes in the mitochondrial compartment.

Discussion

Here, we provide the first transcriptomic analysis across multiple brain regions of an NHP model of MIA. Our findings implicate alterations in transposable element biology, synaptic connectivity, and myelination with relative hippocampal vulnerability in the adolescent NHP brain following MIA. Unexpectedly, strong changes were also detected in V1, which was initially included as a non-psychiatrically relevant comparison region, a finding that warrants further investigation. Although we find no significant overlap between this NHP model and patterns of DE observed in adult patients with SCZ and ASD, these NHPs are significantly younger than human subjects included in genetic and postmortem analysis. Moreover, analysis of the functional pathways implicated by our analysis in the MIA NHP brains are associated with the pathophysiology of both disorders and the magnitude of changes in several co-expression modules correlate with aberrant behaviors. We hypothesize that the transcriptional changes reported here may provide unique insight into prodromal changes in the brain that precede psychosis (70).

MIA has been hypothesized to exert its effect through epigenetic changes which then present dynamically over the trajectory of brain development and maturation (1, 7). Along these lines, multiple studies have reported changes in DNA and histone methylation following MIA (49, 71–74). The most strongly downregulated gene in our dataset, *PIWIL2* is also known to act as a global regulator of DNA methylation through its interactions with piRNAs (44, 45). Thus, if MIA primarily exerts its effect through epigenetic changes, *PIWIL2* may act as a driver of downstream changes. Alternatively, *PIWIL2* may induce changes in gene expression in a secondary manner, by altering regulation of transposable elements, which have shown signs of increased activation in previously published MIA models (72, 74, 75). Changes in transposable elements have been associated with both SCZ and ASD (76, 77), but it is unclear whether and how the complex changes in our NHP MIA dataset are related. Given the increasing appreciation of retrotransposition and other sources of somatic mutations in neurodevelopmental disorders (78–80), these data support an intriguing connection between MIA and this process.

One of the strongest effects of MIA in the brains of adolescent NHPs is altered transcription of genes related to oligodendrocytes and myelination. Consistent with this result, defects in myelination have been reported in other MIA models, as well as in human disease (49, 81–84). This result is broadly in line with the increase in myelination and decrease in neuron projection-related genes observed in adolescent NHPs in this study. All of these studies are limited in ease of comparison due to differences in the timing of MIA exposure. Since altered myelination-related genes have also been reported in both ASD and SCZ (85, 86),

our results highlight the importance of future experiments to determine the progression of MIA-induced changes in myelination through development to adulthood.

Previous MIA studies have shown reproducible behavioral changes in MIA mouse models (87, 88), which have led to a search for a common biological underpinning. Transcriptomic and proteomic studies have examined both embryonic (89–91) and adult (33, 68, 92) timepoints and long-term changes were related to G-protein coupled receptor signaling and glutamatergic and serotonergic receptors, similar to our NHP model. Changes in synaptic connectivity have been hypothesized to be a potential point of convergence for the many diverse genes and biological processes dysregulated in ASD (93, 94). MEdarkgreen, which is downregulated in the DLPFC, contains hub gene *CNTNAP2* which causes a severe recessive neurodevelopmental syndrome associated with hyperactivity, language dysfunction and ASD (95). Additionally, multiple co-expression networks in the hippocampus including MEpaleturquoise, MElightgreen, and MEtan contain genes known to localize in dendritic spines. It is noted that all of these co-expression networks are downregulated, suggesting broad dysregulation at the synapse.

Mitochondria enriched co-expression modules, MEmidnightblue and MEdarkorange, may also provide insights into the behavioral phenotypes in this model. Particularly, both modules from visual cortex (V1) correlate with the number of stereotypies observed in NHPs. There is no known relationship between V1 and repetitive behaviors, so this may reflect more widespread alterations that were only detectable in this region, perhaps because of its high neuronal density (96). Repetitive behaviors are a hallmark of multiple neurodevelopmental and neuropsychiatric illnesses and further assessment of other brain regions that have been associated with repetitive behaviors, such as striatum, is warranted in future studies (97, 98).

While this is a first of its kind study on transcriptomic changes following MIA in NHPs, a few key limitations do exist. First among them is the limited sample size, which is necessitated by the increased costs and longer developmental timeframe when experimenting with NHPs. This combined with the relatively greater genetic diversity among NHP colonies relative to inbred mouse lines may affect the reproducibility of NHP experiments. The smaller samples sizes have also necessitated the use of relatively relaxed statistical thresholds with uncorrected p-values used for co-expression network differential expression and FDR corrected p-values used for gene differential expression and enrichment analyses. These compromises are warranted by the increased genetic and developmental similarities between NHPs and humans, which increases the relevance of findings. We must acknowledge that while reproducibility may be affected, we hope that novel hypotheses generated by this work will lay the foundation for future experiments and justify these statistical thresholds.

Although a broad neural-immune signature was not detected in the brain regions surveyed at this age, that does not preclude the existence of subsets of offspring with and without inflammatory abnormalities which we may be underpowered to detect (35). Future experiments may include the sequencings of samples from additional psychiatrically relevant brain regions (e.g. striatum), females, and additional timepoints, all of which we

limited or are absent in the present study. On a technical note, there are challenges associated with the expression quantification of transposable elements including ambiguity assigning short reads mapping to more than one location (42), and we have observed limited reproducibility between computation pipelines. Therefore, future validations should be performed to gain increased confidence in transposable element results.

These limitations however should not diminish the value of NHP models for understanding the long-term effects of MIA, and the results here should motivate more comprehensive studies in the future. Particularly interesting lines of future work will focus on the role of *PIWIL2* methylation and regulation of transposition in addition to dysregulated myelination trajectories following MIA. Overall, these results provide a starting point for understanding the molecular changes occurring subsequent to MIA during adolescence, a critical period for development of psychosis.

Supplementary Material

Refer to Web version on PubMed Central for supplementary material.

Acknowledgments

References

1. Estes ML, McAllister AK (2015): Immune mediators in the brain and peripheral tissues in autism spectrum disorder. Nat Rev Neurosci. 16: 469–486. [PubMed: 26189694]

2. Hornig M, Bresnahan MA, Che X, Schultz AF, Ukaigwe JE, Eddy ML, et al. (2018): Prenatal fever and autism risk. Mol Psychiatry. 23: 759–766. [PubMed: 28607458]

3. Brucato M, Ladd-Acosta C, Li M, Caruso D, Hong X, Kaczaniuk J, et al. (2017): Prenatal exposure to fever is associated with autism spectrum disorder in the Boston birth cohort. Autism Res. 10: 1878–1890. [PubMed: 28799289]

4. Sørensen HJ, Mortensen EL, Reinisch JM, Mednick SA (2009): Association between prenatal exposure to bacterial infection and risk of schizophrenia. Schizophr Bull. 35: 631–637. [PubMed: 18832344]

5. Nielsen PR, Laursen TM, Mortensen PB (2013): Association between parental hospital-treated infection and the risk of schizophrenia in adolescence and early adulthood. Schizophr Bull. 39: 230–237. [PubMed: 22021661]

6. Khandaker GM, Zimbron J, Lewis G, Jones PB (2013): Prenatal maternal infection, neurodevelopment and adult schizophrenia: a systematic review of population-based studies. Psychol Med. 43.

7. Estes M, McAllister A (2016): Maternal immune activation: Implications for neuropsychiatric disorders. Science 353: 772–777. [PubMed: 27540164]

8. Lichtenstein P, Yip BH, Björk C, Pawitan Y, Cannon TD, Sullivan PF, Hultman CM (2009): Common genetic determinants of schizophrenia and bipolar disorder in Swedish families: a population-based study. Lancet. 373: 234–239. [PubMed: 19150704]

9. Smith SEP, Li J, Garbett K, Mirnics K, Patterson PH (2007): Maternal immune activation alters fetal brain development through interleukin-6. J Neurosci. 27: 10695–10702. [PubMed: 17913903]

10. Careaga M, Murai T, Bauman MD (2017): Maternal Immune Activation and Autism Spectrum Disorder: From Rodents to Nonhuman and Human Primates. Biol Psychiatry. 81: 391–401. [PubMed: 28137374]

11. Meyer U (2014): Prenatal Poly(I:C) Exposure and Other Developmental Immune Activation Models in Rodent Systems. Biol Psychiatry 75: 307–315. [PubMed: 23938317]

12. Knuesel I, Chicha L, Britschgi M, Schobel S, Bodmer M, Hellings J et al. (2014): Maternal immune activation and abnormal brain development across CNS disorders. Nat Rev Neurol 10: 643–660. [PubMed: 25311587]

13. Reisinger S, Khan D, Kong E, Berger A, Pollak A, Pollak D (2015): The Poly(I:C)-induced maternal immune activation model in preclinical neuropsychiatric drug discovery. Pharmacol Therapeut. 149: 213–226.

14. Patterson P (2009): Immune involvement in schizophrenia and autism: Etiology, pathology and animal models. Behav Brain Res. 204: 313–321. [PubMed: 19136031]

15. Richetto J, Calabrese F, Riva M, Meyer U (2013): Prenatal Immune Activation Induces Maturation-Dependent Alterations in the Prefrontal GABAergic Transcriptome. Schizophr Bull. 40: 351–361. [PubMed: 23328159]

16. Hoftman G, Volk D, Bazmi H, Li S, Sampson A, Lewis D (2013): Altered Cortical Expression of GABA-Related Genes in Schizophrenia: Illness Progression vs Developmental Disturbance. Schizophr Bull. 41: 180–191. [PubMed: 24361861]

17. Schmidt M, Mirnics K (2014): Neurodevelopment, GABA System Dysfunction, and Schizophrenia. Neuropsychopharmacology. 40: 190–206. [PubMed: 24759129]

18. Harvey L, Boksa P (2012): A stereological comparison of GAD67 and reelin expression in the hippocampal stratum oriens of offspring from two mouse models of maternal inflammation during pregnancy. Neuropharmacology. 62: 1767–1776. [PubMed: 22178614]

19. Canetta S, Bolkan S, Padilla-Coreano N, Song L, Sahn R, Harrison N et al. (2016): Maternal immune activation leads to selective functional deficits in offspring parvalbumin interneurons. Mol Psychiatry 21: 956–968. [PubMed: 26830140]

20. Wolff A, Bilkey D (2015): Prenatal immune activation alters hippocampal place cell firing characteristics in adult animals. Brain Behav Immun. 48: 232–243. [PubMed: 25843370]

21. Zhang Z, van Praag H (2015): Maternal immune activation differentially impacts mature and adult-born hippocampal neurons in male mice. Brain Behav Immun. 45: 60–70. [PubMed: 25449671]

22. Zuckerman L, Rehavi M, Nachman R, Weiner I (2003): Immune Activation During Pregnancy in Rats Leads to a Postpubertal Emergence of Disrupted Latent Inhibition, Dopaminergic Hyperfunction, and Altered Limbic Morphology in the Offspring: A Novel Neurodevelopmental Model of Schizophrenia. Neuropsychopharmacology. 28: 1778–1789. [PubMed: 12865897]

23. Meyer U, Spoerri E, Yee B, Schwarz M, Feldon J (2008): Evaluating Early Preventive Antipsychotic and Antidepressant Drug Treatment in an Infection-Based Neurodevelopmental Mouse Model of Schizophrenia. Schizophr Bull. 36: 607–623. [PubMed: 18845557]

24. Piontkewitz Y, Assaf Y, Weiner I (2009): Clozapine Administration in Adolescence Prevents Postpubertal Emergence of Brain Structural Pathology in an Animal Model of Schizophrenia. Biol Psychiatry 66: 1038–1046. [PubMed: 19726031]

25. Piontkewitz Y, Arad M, Weiner I (2010): Risperidone Administered During Asymptomatic Period of Adolescence Prevents the Emergence of Brain Structural Pathology and Behavioral Abnormalities in an Animal Model of Schizophrenia. Schizophr Bull. 37: 1257–1269. [PubMed: 20439320]

26. Bauman MD, Iosif A-M, Smith SEP, Bregere C, Amaral DG, Patterson PH (2014): Activation of the maternal immune system during pregnancy alters behavioral development of rhesus monkey offspring. Biol Psychiatry. 75: 332–341. [PubMed: 24011823]

27. Machado CJ, Whitaker AM, Smith SEP, Patterson PH, Bauman MD (2015): Maternal immune activation in nonhuman primates alters social attention in juvenile offspring. Biol Psychiatry. 77: 823–832. [PubMed: 25442006]

28. Bauman MD, Lesh TA, Rowland DJ, Schumann CM, Smucny J, Kukis DL, et al. (2019): Preliminary evidence of increased striatal dopamine in a nonhuman primate model of maternal immune activation. Transl Psychiatry. 9: 135. [PubMed: 30979867]

29. Parikshak NN, Swarup V, Belgard TG, Irimia M, Ramaswami G, Gandal MJ, et al. (2016): Genome-wide changes in lncRNA, splicing, and regional gene expression patterns in autism. Nature. 540: 423–427. [PubMed: 27919067]

30. Gandal MJ, Zhang P, Hadjimichael E, Walker RL, Chen C, Liu S, et al. (2018): Transcriptome-wide isoform-level dysregulation in ASD, schizophrenia, and bipolar disorder. Science. 362. doi: 10.1126/science.aat8127.

31. Richetto J, Chesters R, Cattacneo A, Labouesse M, Gutierrez A, Wood T et al. (2016): Genome-Wide Transcriptional Profiling and Structural Magnetic Resonance Imaging in the Maternal Immune Activation Model of Neurodevelopmental Disorders. Cereb Cortex. doi: 10.1093/cercor/bhw320.

32. Amodeo D, Lai C, Hassan O, Mukamel E, Behrens M, Powell S (2019): Maternal immune activation impairs cognitive flexibility and alters transcription in frontal cortex. Neurobiol Dis. 125: 211–218. [PubMed: 30716470]

33. Weber-Stadlbauer U, Richetto J, Labouesse MA, Bohacek J, Mansuy IM, Meyer U (2017): Transgenerational transmission and modification of pathological traits induced by prenatal immune activation. Mol Psychiatry. 22: 102–112. [PubMed: 27021823]

34. Mattei D, Ivanov A, Ferrai C, Jordan P, Guneykaya D, Buonfiglioli A et al. (2017): Maternal immune activation results in complex microglial transcriptome signature in the adult offspring that is reversed by minocycline treatment. Transl Psychiatry 7: e1120–e1120. [PubMed: 28485733]

35. Purves-Tyson T, Weber-Stadlbauer U, Richetto J, Rothmond D, Labouesse M, Polesel M et al. (2019): Increased levels of midbrain immune-related transcripts in schizophrenia and in murine offspring after maternal immune activation. Mol Psychiatry. doi: 10.1038/s41380-019-0434-0.

36. Bray NL, Pimentel H, Melsted P, Pachter L (2016): Near-optimal probabilistic RNA-seq quantification. Nat Biotechnol. 34: 525–527. [PubMed: 27043002]

37. Robinson MD, McCarthy DJ, Smyth GK (2010): edgeR: a Bioconductor package for differential expression analysis of digital gene expression data. Bioinformatics. 26.

38. Law CW, Chen Y, Shi W, Smyth GK (2014): voom: precision weights unlock linear model analysis tools for RNA-seq read counts. Genome Biol. 15: R29. [PubMed: 24485249]

39. Langfelder P, Horvath S (2008): WGCNA: an R package for weighted correlation network analysis. BMC Bioinformatics. 9: 559. [PubMed: 19114008]

40. Reimand J, Arak T, Adler P, Kolberg L, Reisberg S, Peterson H, Vilo J (2016): g:Profiler—a web server for functional interpretation of gene lists (2016 update). Nucleic Acids Res. 44: W83–W89. [PubMed: 27098042]

41. Skene NG, Grant SGN (2016): Identification of Vulnerable Cell Types in Major Brain Disorders Using Single Cell Transcriptomes and Expression Weighted Cell Type Enrichment. Front Neurosci. 10: 16. [PubMed: 26858593]

42. Criscione SW, Zhang Y, Thompson W, Sedivy JM, Neretti N (2014): Transcriptional landscape of repetitive elements in normal and cancer human cells. BMC Genomics. 15: 583. [PubMed: 25012247]

43. Plaisier SB, Taschereau R, Wong JA, Graeber TG (2010): Rank–rank hypergeometric overlap: identification of statistically significant overlap between gene-expression signatures. Nucleic Acids Res. 38: e169–e169. [PubMed: 20660011]

44. Kuramochi-Miyagawa S, Watanabe T, Gotoh K, Totoki Y, Toyoda A, Ikawa M, et al. (2008): DNA methylation of retrotransposon genes is regulated by Piwi family members MILI and MIWI2 in murine fetal testes. Genes Dev. 22: 908–917. [PubMed: 18381894]

45. Nandi S, Chandramohan D, Fioriti L, Melnick AM, Hébert JM, Mason CE, et al. (2016): Roles for small noncoding RNAs in silencing of retrotransposons in the mammalian brain. Proc Natl Acad Sci USA. doi: 10.1073/pnas.1609287113.

46. Leighton L, Wei W, Marshall P, Ratnu V, Li X, Zajaczkowski E et al. (2019): Disrupting the hippocampal Piwi pathway enhances contextual fear memory in mice. Neurobiol Learn Mem. 161: 202–209. [PubMed: 30965112]

47. Jia L, Liang T, Yu X, Ma C, Zhang S (2013): MGARP Regulates Mouse Neocortical Development via Mitochondrial Positioning. Mol Neurobiol. 49: 1293–1308. [PubMed: 24323429]

48. Li M, Jaffe AE, Straub RE, Tao R, Shin JH, Wang Y, et al. (2016): A human-specific AS3MT isoform and BORCS7 are molecular risk factors in the 10q24.32 schizophrenia-associated locus. Nat Med. 22: 649–656. [PubMed: 27158905]

49. Richetto J, Massart R, Weber-Stadlbauer U, Szyf M, Riva MA, Meyer U (2017): Genome-wide DNA Methylation Changes in a Mouse Model of Infection-Mediated Neurodevelopmental Disorders. Biol Psychiatry. 81: 265–276. [PubMed: 27769567]

50. Meyer U, Nyffeler M, Yee B, Knuesel I, Feldon J (2008): Adult brain and behavioral pathological markers of prenatal immune challenge during early/middle and late fetal development in mice. Brain Behav Immun. 22: 469–486. [PubMed: 18023140]

51. Meyer U, Nyffeler M, Engler A, Urwyler A, Schedlowski M, Knuesel I et al. (2006): The Time of Prenatal Immune Challenge Determines the Specificity of Inflammation-Mediated Brain and Behavioral Pathology. J Neurosci. 26: 4752–4762. [PubMed: 16672647]

52. Rahman T, Weickert C, Harms L, Meehan C, Schall U, Todd J et al. (2020): Effect of Immune Activation during Early Gestation or Late Gestation on Inhibitory Markers in Adult Male Rats. Sci Rep. 10:doi: 10.1038/s41598-020-58449-x.

53. Meehan C, Harms L, Frost J, Barreto R, Todd J, Schall U et al. (2017): Effects of immune activation during early or late gestation on schizophrenia-related behaviour in adult rat offspring. Brain Behav Immun. 63: 8–20. [PubMed: 27423491]

54. Workman AD, Charvet CJ, Clancy B, Darlington RB, Finlay BL (2013): Modeling transformations of neurodevelopmental sequences across mammalian species. J Neurosci. 33: 7368–7383. [PubMed: 23616543]

55. Volk DW, Chitrapu A, Edelson JR, Roman KM, Moroco AE, Lewis DA (2015): Molecular mechanisms and timing of cortical immune activation in schizophrenia. Am J Psychiatry. 172: 1112–1121. [PubMed: 26133963]

56. Amini-Bavil-Olyaee S, Choi YJ, Lee JH, Shi M, Huang I-C, Farzan M, Jung JU (2013): The antiviral effector IFITM3 disrupts intracellular cholesterol homeostasis to block viral entry. Cell Host Microbe. 13: 452–464. [PubMed: 23601107]

57. Ibi D, Nagai T, Nakajima A, Mizoguchi H, Kawase T, Tsuboi D, et al. (2013): Astroglial IFITM3 mediates neuronal impairments following neonatal immune challenge in mice. Glia. 61: 679–693. [PubMed: 23382131]

58. Siegel B, Sengupta E, Edelson J, Lewis D, Volk D (2014): Elevated Viral Restriction Factor Levels in Cortical Blood Vessels in Schizophrenia. Biol Psychiatry 76: 160–167. [PubMed: 24209773]

59. Mi H, Muruganujan A, Ebert D, Huang X, Thomas P (2018): PANTHER version 14: more genomes, a new PANTHER GO-slim and improvements in enrichment analysis tools. Nucleic Acids Res. 47: D419–D426.

60. Mager DL, Hunter DG, Schertzer M, Freeman JD (1999): Endogenous retroviruses provide the primary polyadenylation signal for two new human genes (HHLA2 and HHLA3). Genomics. 59: 255–263. [PubMed: 10444326]

61. Ito J, Sugimoto R, Nakaoka H, Yamada S, Kimura T, Hayano T, Inoue I (2017): Systematic identification and characterization of regulatory elements derived from human endogenous retroviruses. PLoS Genet. 13: e1006883. [PubMed: 28700586]

62. Tam O, Ostrow L, Gale Hammell M (2019): Diseases of the nERVous system: retrotransposon activity in neurodegenerative disease. Mobile DNA 10: . doi: 10.1186/s13100-019-0176-1.

63. Gardner E, Prigmore E, Gallone G, Danecek P, Samocha K, Handsaker J et al. (2019): Contribution of retrotransposition to developmental disorders. Nat Commun 10: . doi: 10.1038/s41467-019-12520-y.

64. Nave K-A, Werner HB (2014): Myelination of the nervous system: mechanisms and functions. Annu Rev Cell Dev Biol. 30: 503–533. [PubMed: 25288117]

65. Renden R, Berwin B, Davis W, Ann K, Chin C, Kreber R et al. (2001): Drosophila CAPS Is an Essential Gene that Regulates Dense-Core Vesicle Release and Synaptic Vesicle Fusion. Neuron 31: 421–437. [PubMed: 11516399]

66. Garay P, Hsiao E, Patterson P, McAllister A (2013): Maternal immune activation causes age- and region-specific changes in brain cytokines in offspring throughout development. Brain Behav Immun. 31: 54–68. [PubMed: 22841693]

67. Giovanoli S, Notter T, Richetto J, Labouesse MA, Vuillermot S, Riva MA, Meyer U (2015): Late prenatal immune activation causes hippocampal deficits in the absence of persistent inflammation across aging. J Neuroinflammation. 12: 221. [PubMed: 26602365]

68. Notter T, Coughlin J, Gschwind T, Weber-Stadlbauer U, Wang Y, Kassiou M et al. (2017): Translational evaluation of translocator protein as a marker of neuroinflammation in schizophrenia. Mol Psychiatry 23: 323–334. [PubMed: 28093569]

69. Winden K, Oldham M, Mirnics K, Ebert P, Swan C, Levitt P et al. (2009): The organization of the transcriptional network in specific neuronal classes. Mol Syst Biol. 5: 291. [PubMed: 19638972]

70. Lieberman J, Small S, Girgis R (2019): Early Detection and Preventive Intervention in Schizophrenia: From Fantasy to Reality. Am J Psychiatry. 176: 794–810. [PubMed: 31569988]

71. Labouesse MA, Dong E, Grayson DR, Guidotti A, Meyer U (2015): Maternal immune activation induces GAD1 and GAD2 promoter remodeling in the offspring prefrontal cortex. Epigenetics. 10: 1143–1155. [PubMed: 26575259]

72. Basil P, Li Q, Dempster EL, Mill J, Sham P-C, Wong CCY, McAlonan GM (2014): Prenatal maternal immune activation causes epigenetic differences in adolescent mouse brain. Transl Psychiatry. 4: e434. [PubMed: 25180573]

73. Connor CM, Dincer A, Straubhaar J, Galler JR, Houston IB, Akbarian S (2012): Maternal immune activation alters behavior in adult offspring, with subtle changes in the cortical transcriptome and epigenome. Schizophr Res. 140: 175–184. [PubMed: 22804924]

74. Basil P, Li Q, Sham P, McAlonan G (2019): LINE1 and Mecp2 methylation of the adult striatum and prefrontal cortex exposed to prenatal immune activation. Data Brief 25: 104003. [PubMed: 31193946]

75. Bundo M, Toyoshima M, Okada Y, Akamatsu W, Ueda J, Nemoto-Miyauchi T, et al. (2014): Increased l1 retrotransposition in the neuronal genome in schizophrenia. Neuron. 81: 306–313. [PubMed: 24389010]

76. Suarez N, Macia A, Muotri A (2017): LINE-1 retrotransposons in healthy and diseased human brain. Dev Neurobiol. 78: 434–455. [PubMed: 29239145]

77. Erwin J, Marchetto M, Gage F (2014): Mobile DNA elements in the generation of diversity and complexity in the brain. Nat Rev Neurosci. 15: 497–506. [PubMed: 25005482]

78. Muotri A, Marchetto M, Coufal N, Oefner R, Yeo G, Nakashima K, Gage F (2010): L1 retrotransposition in neurons is modulated by MeCP2. Nature. 468: 443–446. [PubMed: 21085180]

79. Erwin J, Paquola A, Singer T, Gallina I, Novotny M, Quayle C et al. (2016): L1-associated genomic regions are deleted in somatic cells of the healthy human brain. Nat Neurosci. 19: 1583–1591. [PubMed: 27618310]

80. Lim E, Uddin M, De Rubeis S, Chan Y, Kamumbu A, Zhang X et al. (2017): Rates, distribution and implications of postzygotic mosaic mutations in autism spectrum disorder. Nat Neurosci. 20: 1217–1224. [PubMed: 28714951]

81. Davis K, Stewart D, Friedman J, Buchsbaum M, Harvey P, Hof P et al. (2003): White Matter Changes in Schizophrenia. Arch Gen Psychiatry. 60: 443. [PubMed: 12742865]

82. Scheel M, Prokscha T, Bayerl M, Gallinat J, Montag C (2012): Myelination deficits in schizophrenia: evidence from diffusion tensor imaging. Brain Struct Funct. 218: 151–156. [PubMed: 22327232]

83. Makinodan M, Tatsumi K, Manabe T, Yamauchi T, Makinodan E, Matsuyoshi H, et al. (2008): Maternal immune activation in mice delays myelination and axonal development in the hippocampus of the offspring. J Neurosci Res. 86: 2190–2200. [PubMed: 18438922]

84. Antonson AM, Balakrishnan B, Radlowski EC, Petr G, Johnson RW (2018): Altered Hippocampal Gene Expression and Morphology in Fetal Piglets following Maternal Respiratory Viral Infection. Dev Neurosci. 40: 104–119. [PubMed: 29539630]

85. Hakak Y, Walker J, Li C, Wong W, Davis K, Buxbaum J et al. (2001): Genome-wide expression analysis reveals dysregulation of myelination-related genes in chronic schizophrenia. Proc Natl Acad Sci USA. 98: 4746–4751. [PubMed: 11296301]

86. Graciarena M, Seiffe A, Nait-Oumesmar B, Depino A (2019): Hypomyelination and Oligodendroglial Alterations in a Mouse Model of Autism Spectrum Disorder. Front Cell Neurosci. 12:doi: 10.3389/fncel.2018.00517.

87. Kentner AC, Bilbo SD, Brown AS, Hsiao EY, McAllister AK, Meyer U, et al. (2018): Maternal immune activation: reporting guidelines to improve the rigor, reproducibility, and transparency of the model. Neuropsychopharmacology. doi: 10.1038/s41386-018-0185-7.

88. Meyer U (2019): Neurodevelopmental Resilience and Susceptibility to Maternal Immune Activation. Trends Neurosci. doi: 10.1016/j.tins.2019.08.001.

89. Garbett KA, Hsiao EY, Kálmán S, Patterson PH, Mirnics K (2012): Effects of maternal immune activation on gene expression patterns in the fetal brain. Transl Psychiatry. 2: e98. [PubMed: 22832908]

90. Lombardo MV, Moon HM, Su J, Palmer TD, Courchesne E, Pramparo T (2018): Maternal immune activation dysregulation of the fetal brain transcriptome and relevance to the pathophysiology of autism spectrum disorder. Mol Psychiatry. 23: 1001–1013. [PubMed: 28322282]

91. Oskvig DB, Elkahloun AG, Johnson KR, Phillips TM, Herkenham M (2012): Maternal immune activation by LPS selectively alters specific gene expression profiles of interneuron migration and oxidative stress in the fetus without triggering a fetal immune response. Brain Behav Immun. 26: 623–634. [PubMed: 22310921]

92. Farrelly L, Föcking M, Piontkewitz Y, Dicker P, English J, Wynne K, et al. (2015): Maternal immune activation induces changes in myelin and metabolic proteins, some of which can be prevented with risperidone in adolescence. Dev Neurosci. 37: 43–55. [PubMed: 25592202]

93. Zoghbi H, Bear M (2012): Synaptic Dysfunction in Neurodevelopmental Disorders Associated with Autism and Intellectual Disabilities. Cold Spring Harb Perspect Biol. 4: a009886–a009886. [PubMed: 22258914]

94. Bourgeron T (2015): From the genetic architecture to synaptic plasticity in autism spectrum disorder. Nat Rev Neurosci. 16: 551–563. [PubMed: 26289574]

95. Rodenas-Cuadrado P, Ho J, Vernes S (2013): Shining a light on CNTNAP2: complex functions to complex disorders. Eur J Hum Genet. 22: 171–178. [PubMed: 23714751]

96. Collins C, Airey D, Young N, Leitch D, Kaas J (2010): Neuron densities vary across and within cortical areas in primates. Proc Natl Acad Sci USA. 107: 15927–15932. [PubMed: 20798050]

97. Militerni R, Bravaccio C, Falco C, Fico C, Palermo M (2002): Repetitive behaviors in autistic disorder. Eur Child Adoles Psy. 11: 210–218.

98. Langen M, Bos D, Noordermeer S, Nederveen H, van Engeland H, Durston S (2014): Changes in the Development of Striatum Are Involved in Repetitive Behavior in Autism. Biol Psychiatry 76: 405–411. [PubMed: 24090791]
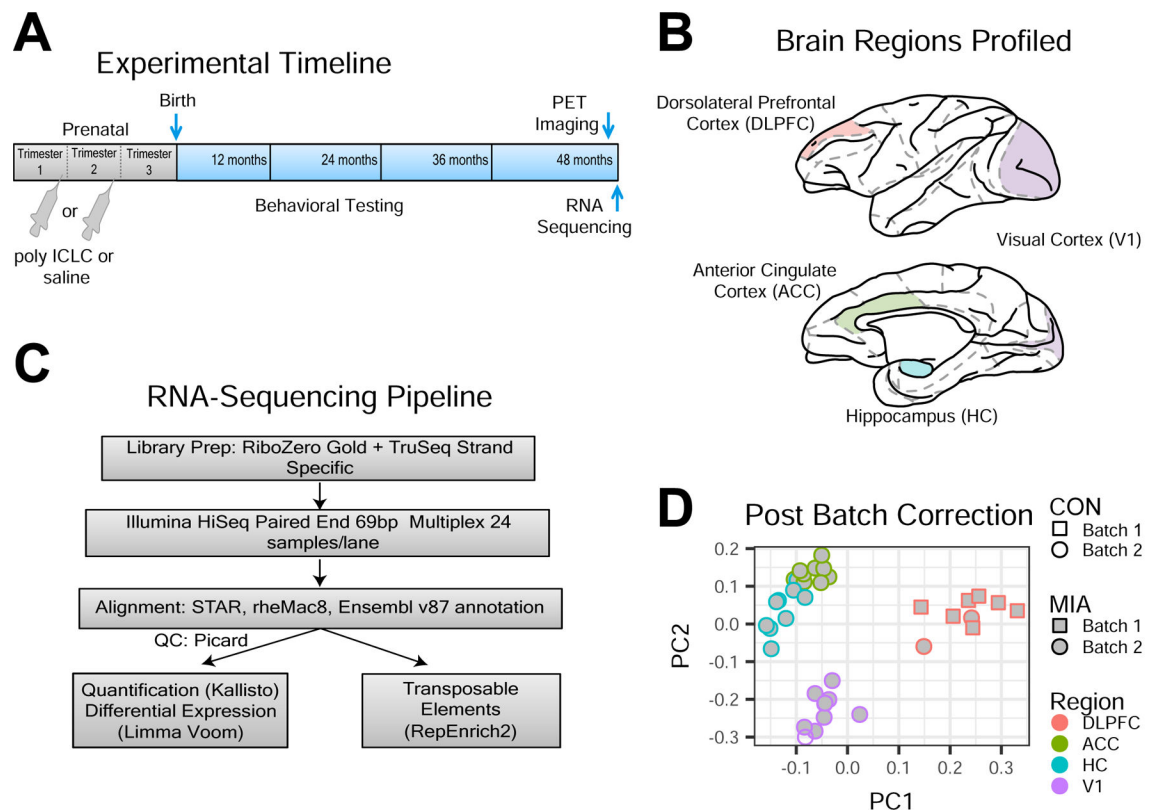
Figure 1.
Outline of experimental approach and bioinformatic analyses. **(A)** Female non-human primates were injected with the viral mimic Poly:ICLC once daily for 3 days starting at gestational day GD44 (1st Trimester MIA) or GD101 (2nd Trimester MIA; see Methods and Materials for details). Tissue was harvested from male offspring at 48 months followed by RNA-sequencing. Behavioral testing for stereotypic behaviors was performed throughout development and PET imaging was performed directly before sequencing and has been previously published on this same cohort (27). **(B)** Brain regions with relevance to schizophrenia and autism biology were profiled including dorsolateral prefrontal cortex (DLPFC), cingulate cortex (ACC), and hippocampus (HC) with primary visual cortex (V1) also included for comparison. **(C)** Diagram of RNA-sequencing pipeline. Briefly, RiboZero strand specific library preparation was performed before obtaining 69bp paired end Illumina reads. Reads were aligned to the current version of the Rhesus genome and quantified with Kallisto or RepEnrich2, which is specially designed to detect the expression of transposable elements (TEs). In both cases differential expression was quantified using a linear mixed effects model with Limma-voom. **(D)** Top principal components (PCs) of normalized gene expression demonstrating that batch and brain region are the largest drivers of variation in the dataset.
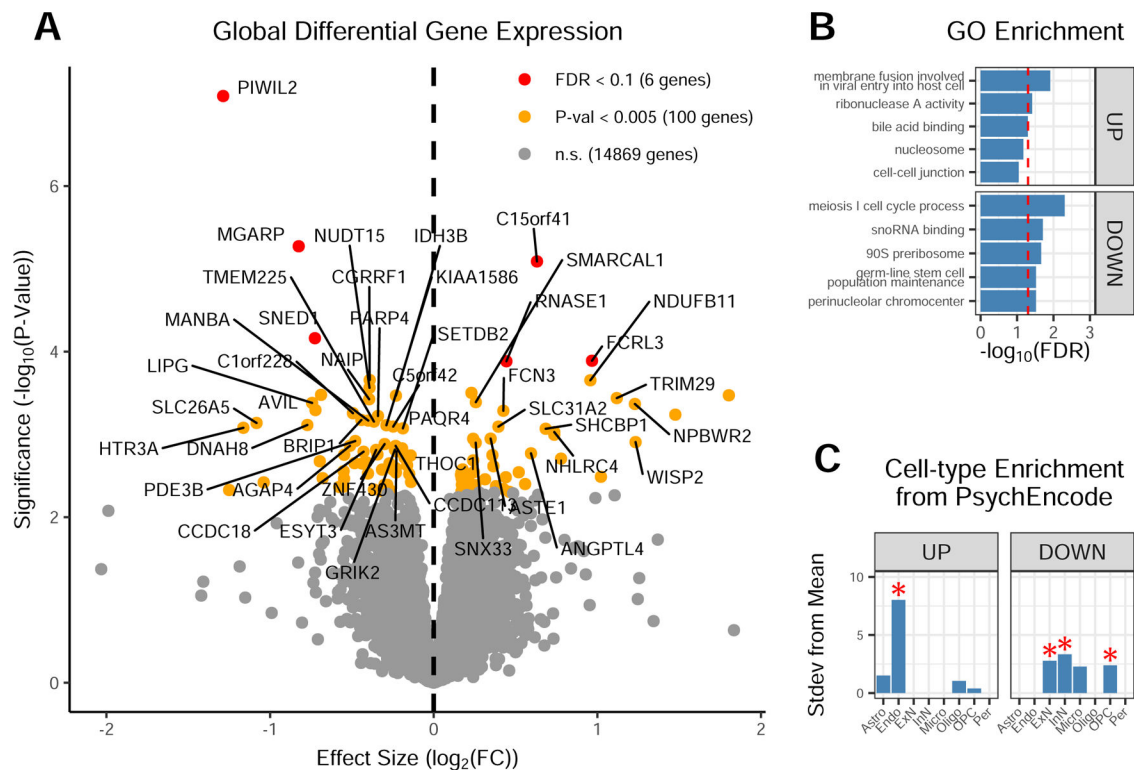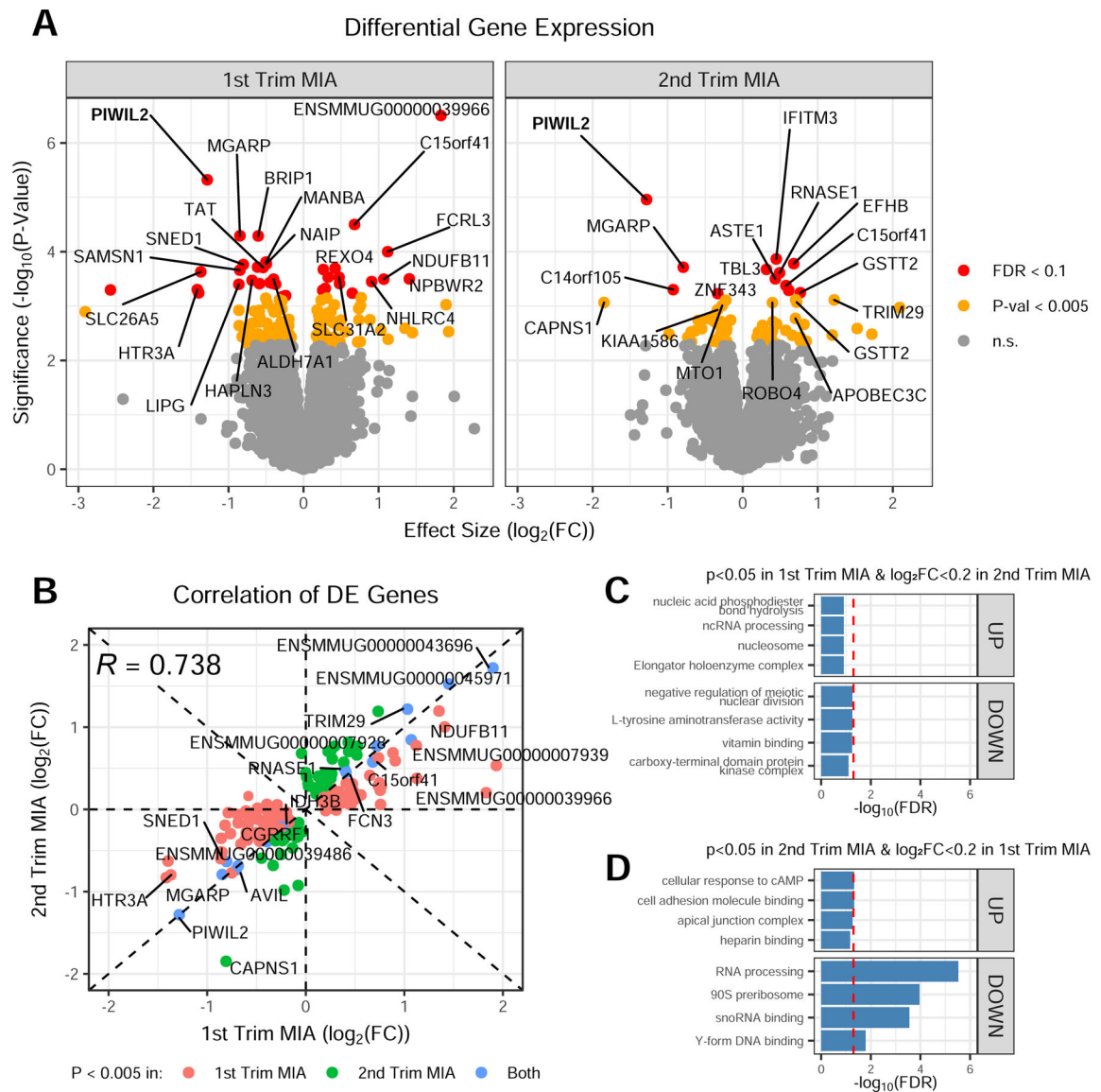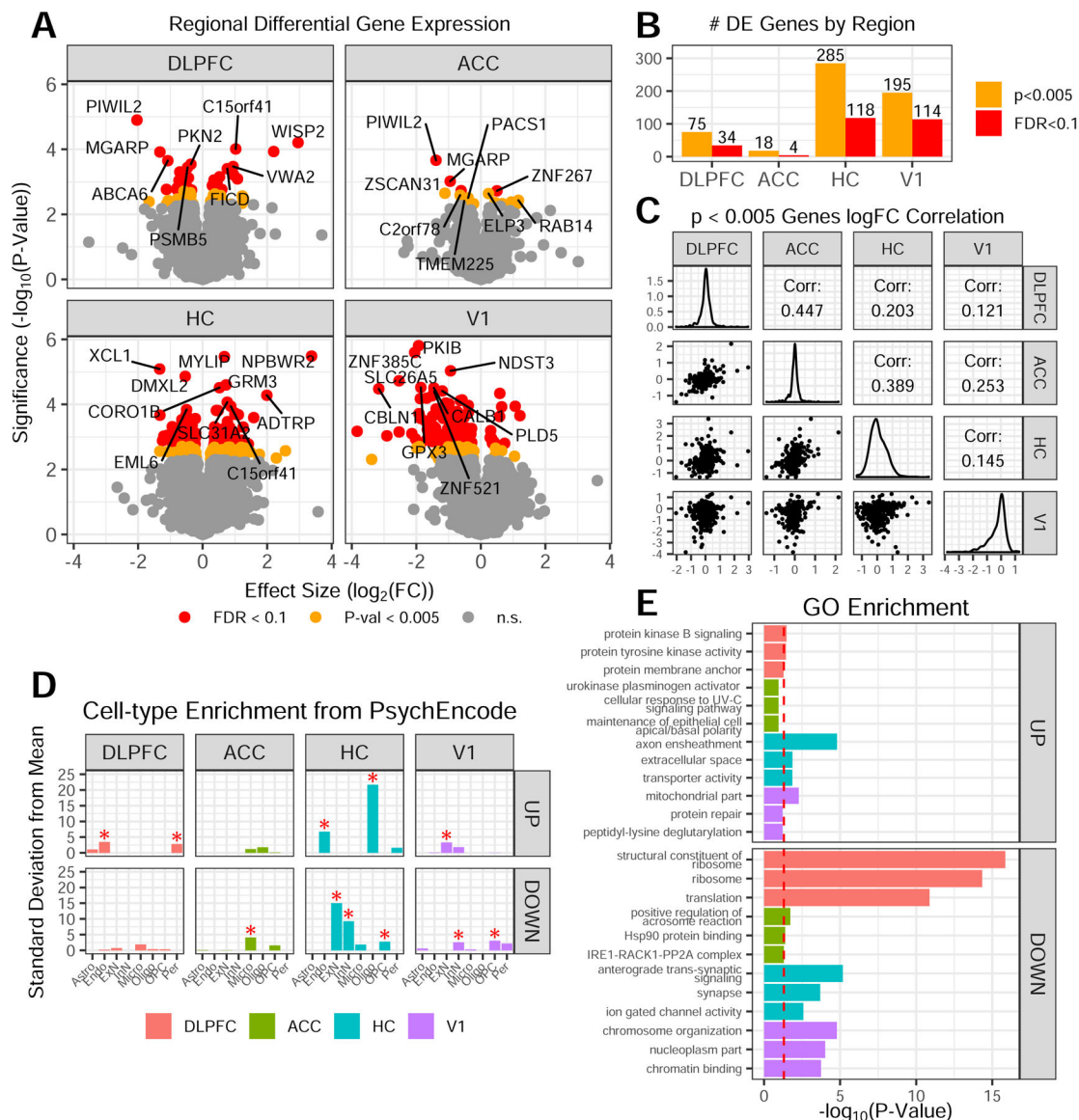
Figure 2.
Global differential gene expression across brain regions following MIA. **(A)** Differential gene expression analysis using Limma-voom was performed on all saline injected vs. poly:ICLC injected MIA samples and pooled across brain regions and MIA timepoints. Volcano plot of differential gene expression detects *PIWIL2* as the top globally downregulated gene followed by *MGARP*. Red dots indicate genes that pass FDR correction for differential gene expression (FDR<0.1), yellow dots indicate suggestive association with MIA, and grey dots indicate minimal or no association. Dotted line indicates $\log_2(FC)=0$. Genes are labelled according to their human homologs, those without annotated homologs are left unlabeled. **(B)** Top GO terms enriched among up and downregulated genes with p<0.05 following MIA determined using g:ProfileR. Red dotted line indicates an FDR significance threshold of 0.05. **(C)** Cell-type specificity of up and downregulated genes following MIA with p<0.05 genes based on PsychEncode and Lake et al., 2018 adult human single-cell Nuc-seq data. *FDR<0.05, unlabeled cell-types are not significantly enriched.

Figure 3.
High concordance between genes differentially expressed in first and second trimester MIA offspring. **(A)** Differential gene expression analysis using Limma-voom was performed separately on saline injected vs. poly:ICLC injected MIA samples from 1st or 2nd trimester pooled across brain regions. Volcano plots of differential gene expression detect *PIWIL2* and *MGARP* as the top downregulated genes following both 1st and 2nd trimester MIA. Red dots indicate genes that pass FDR correction for differential gene expression (FDR<0.1), yellow dots indicate suggestive association with MIA, and grey dots indicate minimal or no association. Genes are labelled according to their human homologs, those without annotated homologs are left unlabeled. **(B)** All genes with suggestive association with MIA p<0.005 following either timepoint of poly:ICLC injection were plotted comparing their log2(FC) following either 1st or 2nd trimester MIA. Blue dots indicate genes that are associated with MIA regardless of timepoint while red and green dots indicate specific dysregulation following 1st or 2nd trimester MIA respectively. The overall log2(FC) correlation between

genes dysregulated following either timepoint is R=0.738. **(C, D)** To determine the trimester specific effects of MIA, GO enrichment was determined for genes with p<0.05 following 1st trimester MIA and $\log_2$(FC)<0.2 following 2nd trimester MIA and vise-versa using g:ProfileR. Red dotted line indicates an FDR significance threshold of 0.05.

Figure 4.
MIA alters gene expression in a region-specific manner in the brains of offspring. **(A)** Differential gene expression analysis using Limma-voom was performed separately for each brain region on all saline injected vs. poly:ICLC injected MIA samples pooled across MIA timepoints. Volcano plots indicate the top 10 differentially expressed genes in each region following MIA. Red dots indicate genes that pass FDR correction for differential gene expression (FDR<0.1), yellow dots indicate suggestive association with MIA, and grey dots indicate minimal or no association. Genes are labelled according to their human homologs, those without annotated homologs are left unlabeled. **(B)** The number of DE genes in each region by significance threshold. **(C)** log$_2$(FC) of all genes with suggestive association (p<0.005) with MIA in at least one brain region are compared pairwise with each other brain region. Small correlations indicate minimal overlap in the similarity of gene expression changes between each region following MIA. **(D)** Cell-type specificity of region specific up

and downregulated genes following MIA with p<0.05 genes based on PsychEncode and Lake et al., 2018 adult human single-cell Nuc-seq data. ***FDR<0.05**, unlabeled cell-types are not significantly enriched. **(E)** Top GO terms enriched among region specific up and downregulated genes with p<0.05 following MIA determined using g:ProfileR. Red dotted line indicates an FDR significance threshold of 0.05.
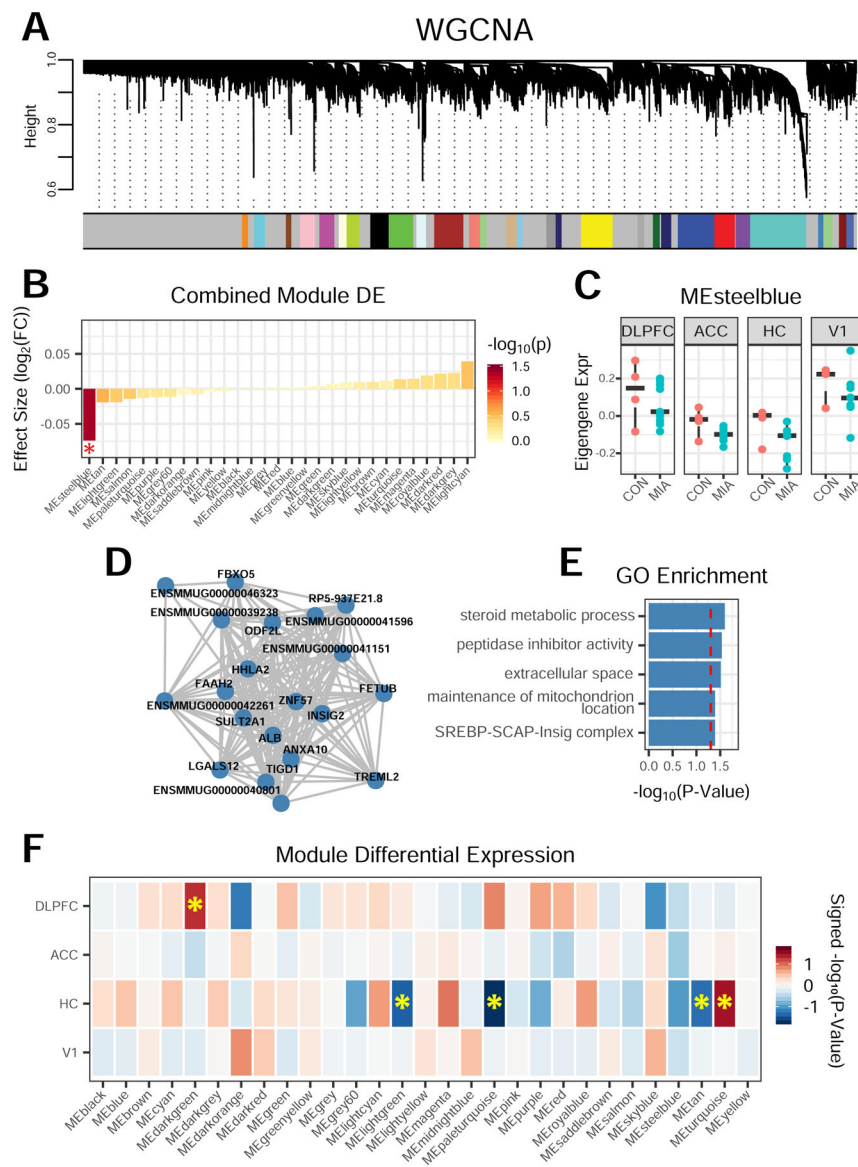
Figure 5.

Consistent changes across brain regions in MIA offspring implicates transposable elements and steroid biology. **(A)** WGCNA was used to construct a signed bicor network and identify co-expression network modules, each containing genes whose expression is highly correlated across samples. Dendrotree height indicates the degree of co-expression correlation and colors indicate co-expression network module assignments. **(B)** Differential co-expression network expression was determined using Limma-lmFit on all saline injected vs. poly:ICLC injected MIA samples pooled across brain regions and MIA timepoints. Only one co-expression network, MEsteelblue, is significantly downregulated across all pooled samples. *p<0.05. **(C)** Boxplot of MEsteelblue module eigengene expression across the brain regions analyzed. **(D)** Top 20 hub genes for MEsteelblue. **(E)** Top GO terms enriched in MEsteelblue region by g:ProfileR. For all GO enrichment plots, red dotted line indicates an FDR significance threshold of 0.05. **(F)** Differential module expression was determined

using Limma-lmFit separately for each brain region on all saline injected vs. poly:ICLC injected MIA samples pooled across MIA timepoints. **p<0.05.
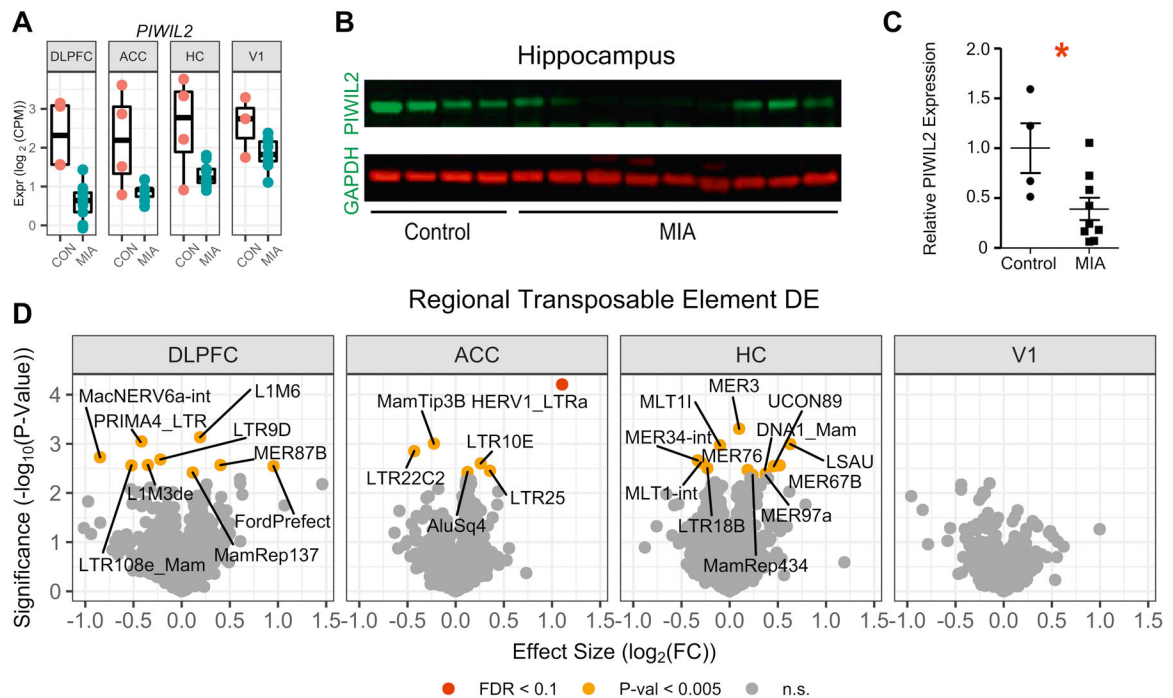
Figure 6.
MIA causes dysregulation of transposable elements across brain regions in offspring. **(A)**
Boxplot of piRNA regulator *PIWIL2* expression across brain regions following MIA. **(B)**
Western blot of PIWIL2 expression on the hippocampus following MIA. Blot was
performed only once due to limited sample availability (Control, n=4; MIA, n=9). **(C)**
Quantification of part B relative to GAPDH. *p<0.05. **(D)** Differential transposable element
expression analysis using Limma-voom was performed separately for each brain region on
all saline injected vs. poly:ICLC injected MIA samples pooled across MIA timepoints.
Volcano plots indicate all transposable elements with suggestive association with MIA in
each brain region. Red dots indicate transposable elements that pass FDR correction for
differential transposable elements expression (FDR<0.1), yellow dots indicate suggestive
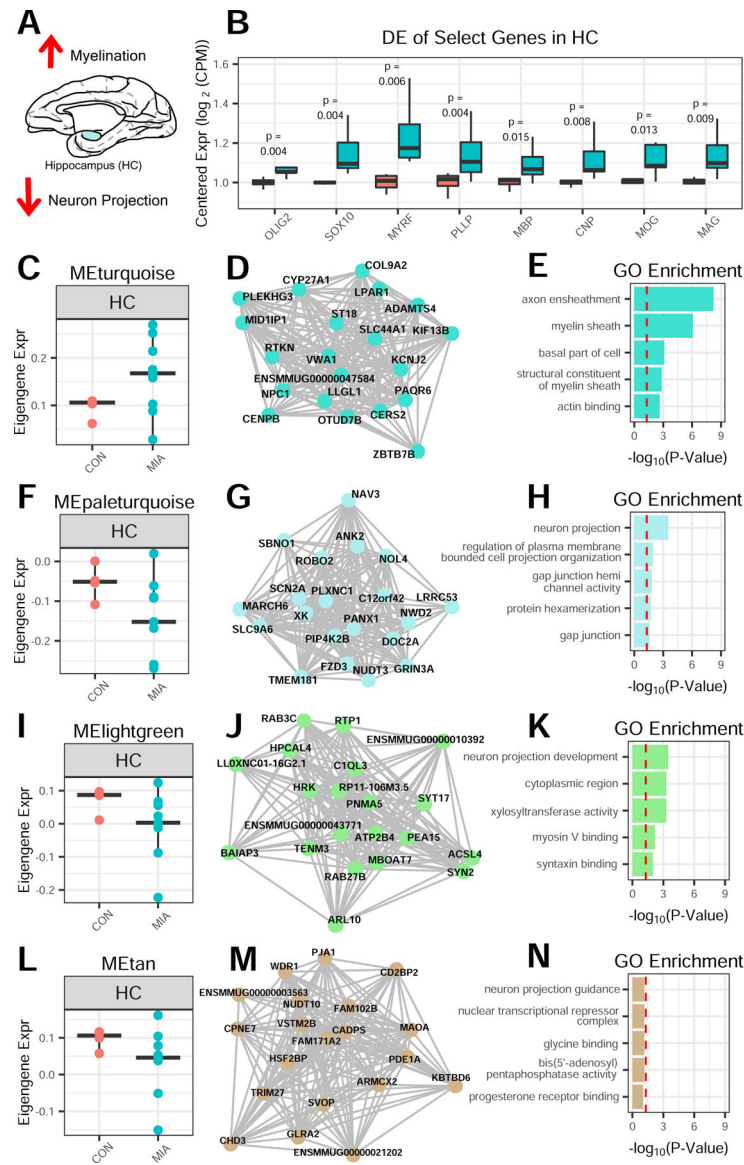association with MIA, and grey dots indicate minimal or no association.

Figure 7.

MIA increases myelination and oligodendrocyte-related genes and decreases neuron projection genes in hippocampus of offspring. **(A)** Summary of changes in the HC. **(B)** Multiple oligodendrocyte and myelin sheath related genes are upregulated in the HC following MIA. **(C)** Boxplot of MEturquoise module eigengene expression across the brain regions analyzed. **(D)** Top 20 hub genes for MEturquoise. **(E)** Top GO terms enriched in MEturquoise region by g:ProfileR. **(F)** Boxplot of MEpaleturquoise module eigengene expression across the brain regions analyzed. **(G)** Top 20 hub genes for MEpaleturquoise. **(H)** Top GO terms enriched in MEpaleturquoise region by g:ProfileR. **(I)** Boxplot of MElightgreen module eigengene expression across the brain regions analyzed. **(J)** Top 20 hub genes for MElightgreen. **(K)** Top GO terms enriched in MElightgreen region by g:ProfileR. **(L)** Boxplot of MEtan module eigengene expression across the brain regions analyzed. **(M)** Top 20 hub genes for MEtan. **(N)** Top GO terms enriched in MEtan region by

g:ProfileR. For all GO enrichment plots, red dotted line indicates an FDR significance threshold of 0.05.
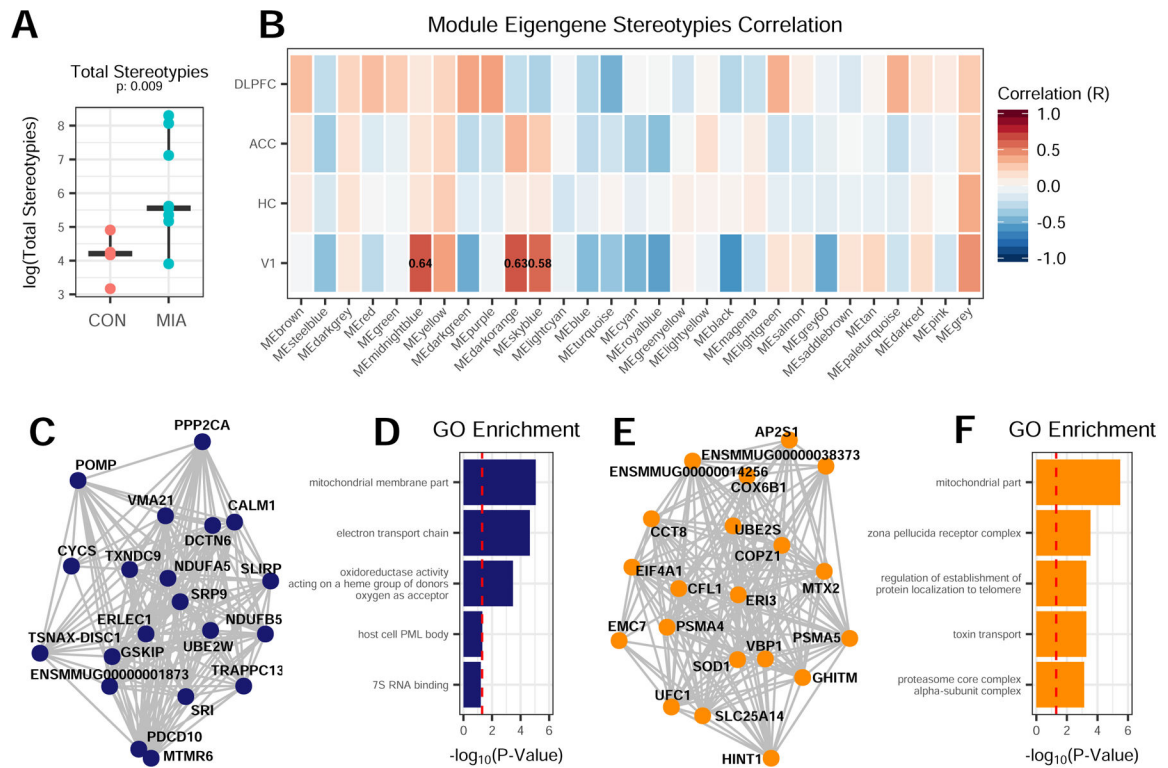
Figure 8.

Mitochondrial co-expression networks in V1 correlate with behavioral aberrations in offspring. **(A)** The total number of stereotypic behaviors was measured in NHPs throughout development. The $\log_2$(Total # stereotypies) observed is significantly increased in MIA offspring as compared to controls (p=0.009; Student's t-test). **(B)** Correlation between module eigengene expression in a given region and the $\log_2$(Total # stereotypies) in a given subject. The largest correlations with $\log_2$(Total # stereotypies) are found in V1, particularly MEmidnightblue and MEdarkorange. **(C)** Top 20 hub genes for MEmidnightblue **(D)** Top GO terms enriched in MEmidnightblue by g:ProfileR. **(E)** Top 20 hub genes for MEdarkorange **(F)** Top GO terms enriched in MEdarkorange by g:ProfileR. For all GO enrichment plots, red dotted line indicates an FDR significance threshold of 0.05.

KEY RESOURCES TABLE

Resource Type	Specific Reagent or Resource	Source or Reference	Identifiers	Additional Information
Add additional rows as needed for each resource type	Include species and sex when applicable.	Include name of manufacturer, company, repository, individual, or research lab. Include PMID or DOI for references; use "this paper" if new.	Include catalog numbers, stock numbers, database IDs or accession numbers, and/or RRIDs. RRIDs are highly encouraged; search for RRIDs at https://scicrunch.org/resources.	Include any additional information or notes if necessary.
Antibody	Mouse monoclonal anti-GAPDH	Sigma-Aldrich	Cat# G8795, RRID:AB_1078991	
Antibody	Sheep polyclonal anti-PIWIL2	R&D Biosciences	Cat# AF6558, RRID:AB_10718706	
Antibody	Rabbit polyclonal anti-CX3CR1	Sigma-Aldrich	Cat# C8354, RRID:AB_259103	
Antibody	Rabbit polyclonal anti-IGSF6	Atlas Antibodies	Cat# HPA041072, RRID:AB_10794262	
Biological Sample	Male non-human primate (Macaca mulatta) brain tissue	Bauman et al., 2014 (https://pubmed.ncbi.nlm.nih.gov/24011823/)	DOI: 10.1016/j.biopsych.2013.06.025	
Biological Sample	Maternal (female) non-human primate (Macaca mulatta) blood samples	Bauman et al., 2014 (https://pubmed.ncbi.nlm.nih.gov/24011823/)	DOI: 10.1016/j.biopsych.2013.06.025	
Commercial Assay Or Kit	Monkey IL-6 ELISA Kit	Cell Sciences	Cat# CKM005	
Commercial Assay Or Kit	Non-human primate multiplexing bead immunoassay	Milipore-Sigma	Cat# PCYTMG-40K-PX23	
Commercial Assay Or Kit	miRNeasy Mini Kit	Qiagen	Cat# 217004	
Commercial Assay Or Kit	TruSeq® Stranded Total RNA Library Prep Gold	Illumina	Cat# 20020599	
Deposited Data; Public Database	Rhesus Macaque (Macaca mulatta) reference genome (rheMac8)	UCSC Genome Browser (http://hgdownload.soe.ucsc.edu/goldenPath/rheMac8/bigZips/)	https://www.ncbi.nlm.nih.gov/assembly/GCF_000772875.2/	
Deposited Data; Public Database	Macaque Ensembl v87 annotations	Ensembl Archive	ftp://ftp.ensembl.org/pub/release-87/gtf/macaca_mulatta/	
Deposited Data; Public Database	SFARI gene list (Scores 1 & 2 only)	SFARI Gene Archive	https://gene-archive.sfari.org/database/gene-scoring/	
Deposited Data; Public Database	PsychEncode differential expression data	Gandal et al., 2018 (https://pubmed.ncbi.nlm.nih.gov/30545856/)	DOI: 10.1126/science.aat8127	
Deposited Data; Public Database	PsychEncode + Lake et al., 2018 Nuc-Seq data	PsychEncode; Lake et al., 2018 (https://www.ncbi.nlm.nih.gov/pmc/articles/PMC5951394/)	http://resource.psychencode.org/	
Organism/Strain	Rhesus Macaque	California National Primate Research Center	Macaca mulatta	
Software; Algorithm	Bioplex Manager Software	Bio-Rad	RRID:SCR_014330	
Software; Algorithm	STAR v2.5.0a	Dobin et al., 2013 (https://pubmed.ncbi.nlm.nih.gov/23104886/)	RRID:SCR_015899	

Resource Type	Specific Reagent or Resource	Source or Reference	Identifiers	Additional Information
Add additional rows as needed for each resource type	**Include species and sex when applicable.**	**Include name of manufacturer, company, repository, individual, or research lab. Include PMID or DOI for references; use "this paper" if new.**	**Include catalog numbers, stock numbers, database IDs or accession numbers, and/or RRIDs. RRIDs are highly encouraged; search for RRIDs at https://scicrunch.org/resources.**	**Include any additional information or notes if necessary.**
Software; Algorithm	kallisto	Bray et al., 2016 (https://pubmed.ncbi.nlm.nih.gov/27043002/)	RRID:SCR_016582	
Software; Algorithm	tximport	Soneson et al., 2015 (https://pubmed.ncbi.nlm.nih.gov/26925227/)	RRID:SCR_016752	
Software; Algorithm	Picard	Broad Institute (http://broadinstitute.github.io/picard/)	RRID:SCR_006525	
Software; Algorithm	edgeR	Robinson et al., 2010 (https://pubmed.ncbi.nlm.nih.gov/19910308/)	RRID:SCR_012802	
Software; Algorithm	Limma-voom	Law et al., 2014 (https://pubmed.ncbi.nlm.nih.gov/24485249/)	RRID:SCR_010943	
Software; Algorithm	WGCNA	Langfelder and Horvath, 2008 (https://pubmed.ncbi.nlm.nih.gov/19114008/)	RRID:SCR_003302	
Software; Algorithm	RepErich2	Criscione et al., 2014 (https://pubmed.ncbi.nlm.nih.gov/25012247/)	NA	
Software; Algorithm	G:profileR	Reimand et al., 2007 (https://www.ncbi.nlm.nih.gov/pmc/articles/PMC1933153/)	RRID:SCR_006809	
Software; Algorithm	EWCE	Skeene and Grant, 2016 (https://pubmed.ncbi.nlm.nih.gov/26858593/)	NA	
Software; Algorithm	RRHO	Plaisier et al., 2010 (https://pubmed.ncbi.nlm.nih.gov/20660011/)	RRID:SCR_014024	
Software; Algorithm	Image Studio Software	LI-COR	RRID:SCR_015795	
Software; Algorithm	GraphPad Prism	Graphpad	RRID:SCR_002798	
Other	poly:ICLC	Oncovir, Inc.	NA	
Other	Bio-Plex® 200 System	Bio-Rad	Cat# 171000201	
Other	Odyssey® CLx Imaging System	LI-COR	https://www.licor.com/bio/odyssey-clx/index	